SIMULATION OF PARTICLE FLUXES AND COSMOGENIC NUCLIDE PRODUCTION IN THE EARTH'S ATMOSPHERE

J. Masarik[1] and J. Beer

EAWAG, CH-8600 Duebendorf, Switzerland

Will be published in:
Journal of Geophysical Research, **D104** (10), 12,099-13,012, (1999).

[1] Permanent address: Space Sciences Laboratory, University of California, Berkeley, Ca 94720, USA and

Simulation of particle fluxes and cosmogenic nuclide production in the Earth's atmosphere

J. Masarik[2] and J. Beer

Environmental Physics,, Swiss Federal Institute of Environmental Science and Technology, Duebendorf, Switzerland

Abstract. A purely physical model for the simulation of cosmic ray particle interactions with the Earth's atmosphere and subsequent production and transport of secondary particles is presented. Neutron and proton spectra as a function of the coordinate in the atmosphere were calculated using a GEANT / MCNP-based code system. The calculated neutron fluxes are in good agreement with experimental data based on neutron monitor measurements. These fluxes, together with experimental or evaluated cross sections, were used to calculate the production rates of ^{3}H, ^{7}Be, ^{10}Be ^{14}C, and ^{36}Cl. The dependencies of these production rates on solar activity and geomagnetic field intensity were investigated in detail. The obtained production rates agree well with most published experimental and theoretical values. Possible reasons for some differences are discussed.

1. Introduction

The interactions of cosmic ray particles with the Earth's atmosphere produce a cascade of secondary particles and a variety of cosmogenic nuclides. The development of accelerator mass spectrometry (AMS) has increased the detection sensitivity for long-lived cosmogenic radionuclides by several orders of magnitude and allows us now to analyze with high-resolution natural archives such as ice cores. The concentration of cosmogenic nuclides in these archives is the result of the interplay between three processes: production, transport, and deposition. In order to make full use of the information stored in these archives, a detailed knowledge of the source functions of the cosmogenic nuclides is necessary. After production the nuclides are subject to different processes according to their geochemical properties. For example, ^{14}C is oxidized to CO_2, and ^{10}Be becomes attached to aerosols. Then they are distributed from the site of their creation following the trajectories of the air masses until, finally, part of them become stored in natural archives. Because of the thermal structure of the stratosphere and its separation from the troposphere by the tropopause, the residence time of aerosols in the stratosphere is about 1-2 years. In the troposphere the residence time is substantially shorter, only in the order of weeks. The concentration of the cosmogenic nuclides at a specific site is strongly dependent on the local precipitation rate.

Models have to be developed that describe the production of nuclides by the interaction of cosmic ray particles with the main target elements of the atmosphere and their subsequent transport from the atmosphere into the various archives. The main purpose of this paper is to establish a new theoretical model for the simulation of processes relevant in cosmogenic nuclide production. Lacking reliable nuclear models and cross sections, the first extensive and pioneering work in this field by *Lal and Peters* [1967] was based on data from direct observations limited to a few years. Subsequently, there have been a number of model calculations devoted to particle and cosmogenic nuclide production in the atmosphere [*Hess et al.,* 1961*; Newkirk,* 1963*; Lingenfelter, 1963; Oeschger et al.,* 1969*; Light et al.,* 1973*; O'Brien,* 1979*; Blinov,* 1988*; Masarik and Reedy,* 1995]. The relatively good agreement between the calculated and measured ^{14}C production rates proved the reliability of the model approach.

Technical developments like satellites and AMS now are generating enormous amounts of new data. Among the data are fluxes of cosmic ray particles, detailed information about solar flares, energetic and isotopic composition of cosmic rays, properties and characteristics of the Earth's atmosphere etc. On the basis of this data, new theories on the role of cosmic ray particles in the atmosphere were formulated [Tinsley et al., 1989; Svensmark and Friis-Christensen, 1997]. However, in many of the phenomena that are presently under investigation, the involved time constants are much longer than a few years. Therefore we need additional information corresponding to dif-ferent times in the past, that can be characterized by condi-tions that differ significantly from the present ones (quiet-Sun peri-ods like during the Wolf (1280-1350 AD), Sporer (1420-1540 A.D.) or Maunder (1645-1715 A.D.) minima; low or high geomagnetic field intensity like during the Laschamp event about 40 Ky B.P.).

The production rate of cosmogenic nuclides depends on the cosmic ray particle flux. Time-dependent changes of the production rate are caused mainly by variations of the geomagnetic field intensity and the solar activity. From measurements of cosmogenic radionuclides with different half-lives and different irradiation histories in meteorites, the average galactic cosmic ray flux was inferred to be constant within 10% during the last few million years [*Vogt et al.,* 1990]. In the investigation of temporal variations of cosmic ray intensity in the past, using cosmogenic nuclides produced in extraterrestrial and terrestrial samples, one has to account for important differences in their archives: most of the extraterrestrial records integrate cosmic ray effects over different periods

of time determined by the half-life of the radionuclide and the exposure age, while most of the terrestrial records are differential, often representing only a very small window of time in the past. The incident cosmic ray flux on Earth is different from that incident on meteorites at least in one respect: the Earth's geomagnetic field prevents most low-energy cosmic ray particles from interacting with the atmosphere.

Solar modulation is the dominant cause of the observed galactic cosmic ray (GCR) variability. Near the Earth during a typical solar cycle, the low-energy part of GCR particle flux (E < 1 GeV nucleon^{-1}) varies by an order of magnitude. With increasing energy, the modulation effect becomes weaker. The modulation is caused by the interaction of incoming GCR particles with magnetic fields convected outward by the solar wind plasma, which leads to scattering, diffusions and energy losses. The modulation effects take place in a region as large as 100 AU, the heliosphere. Measurements of the fluxes of GCR particles using experiments on balloons, satellites, and Earth-surface-based neutron monitors have shown that the modulation processes are complicated and cannot be described simply by an anticorrelation with solar activity [*Garcia-Munoz et al.*, 1977].

The geomagnetic field, which is dominated by its dipole component, also acts as a shield. It deflects incoming particles depending on their electric charge, energy, and angle of incidence. Depending on the geomagnetic latitude and angle of incidence, there is a critical energy below which cosmic ray particles cannot penetrate into the Earth's atmosphere. This leads to a latitudinal dependence of the primary and secondary particle fluxes and consequently also of the production rate of cosmogenic nuclides, with higher values around the magnetic poles and lower values in the equatorial region. From paleomagnetic records, it is known that the geomagnetic field varied in the past in its intensity, direction, and polarity [*Tauxe*, 1985*; Gosse et al.*, 1996].

Concentrations of cosmogenic nuclides observed in various archives on the Earth's surface are determined by their production, atmospheric mixing, and deposition processes. We concentrate our attention in this paper only on the production processes. Besides the latitude, the production rate depends also on the altitude. Primary cosmic rays incident on the top of the atmosphere consist mainly of protons with energies around 1 GeV. The characteristic feature of nuclear interactions at these energies is the production of secondary particles, many of, which have enough energy to undergo further collisions in the atmosphere and contribute to the development of a particle cascade. The development of this cascade process leads to a decrease of the primary cosmic-ray particle flux and a strong increase of the number of secondary particles with increasing atmospheric depth. After production of several generations of particles, the cascade process ends when the energies of the particles become too low for further particle production. On the basis of these features of particle cascade development, one expects that the production rate begins to increase at the top of the atmosphere, reaches a maximum at a depth between 100 - 200 g cm^{-2} depending on nuclide and latitude), and finally decreases gradually down to the Earth's surface.

To simulate in detail the development of the cascade and to calculate the corresponding production rates of cosmogenic isotopes in the atmosphere, the GEANT [*Brun et al.*, 1987] and MCNP [*Briesmeister, 1993*] code systems were applied. These codes use only basic physical quantities and parameters, without including any free parameters, to numerically simulate all processes relevant in particle production and transport. This enables us to trace the fate of each individual particle and in doing so to study in detail the effects of various parameters on the production rate, such as geomagnetic and solar modulation, for a wide range of possible conditions. Our present work is an extension of previous calculations [*Masarik and Reedy*, 1995] carried out with the LAHET Code System (LCS) [*Prael and Lichtenstein*, 1989], part of which is also MCNP. The LCS model has been previously tested for the special case of experimental production rates in extraterrestrial objects [*Reedy et al.*, 1993*; Masarik and Reedy*, 1994*; Reedy and Masarik*, 1994]. All the tests showed good agreement between experimental data and calculations, which confirms the validity of this model. After replacing LAHET by GEANT, some of the extraterrestrial simulations were repeated. Within the statistical errors, an equally good agreement between experimental and calculated production rates was obtained.

2. Calculation Model

2.1. Calculation of Cosmogenic Nuclide Production Rates

The production rate of the cosmogenic nuclide j at depth D is

$$P_j(D) = \sum_i N_i \sum_k \int_0^\infty \sigma_{ijk}(E_k)\ J_k(E_k, D) dE_k \qquad (1)$$

where N_i is the number of atoms for target element i per kg material in the sample, $\sigma_{ijk}(E_k)$ is the cross section for the production of nuclide j from the target element i by particles of type k with energy E_k, and $J_k(E_k,D)$ is the total flux of particles of type k with energy E_k at location D inside the atmosphere. In our model, the particle fluxes $J_k(E_k,D)$ are calculated using the GEANT and MCNP codes. The cross sections $\sigma_{ijk}(E_k)$ were those evaluated from many measurements and used in earlier calculations. Details related to the used cross sections are given in section 2.6. The basics of the physical models implemented in the codes are presented below.

While codes like GEANT and MCNP can calculate production rates of nuclides directly, we believe that such codes can do better in calculating the particle fluxes rather than the produced nuclides. This statement is due to the fact that these codes use only well-known particle-particle cross sections for the calculation of particle fluxes. Therefore the calculated secondary particle fluxes are expected to be fairly accurate. The problems related with the direct calculation of production rates are summarized in *Masarik and Reedy* [1994]. The main problem with the calculation of production rates using calculated fluxes and code-independent sets of cross sections for the particular nuclides is the frequent lack of measured cross sections, especially for neutron-induced

reactions. A similar approach based on a combination of thin-target cross sections with calculated particle fluxes was used by *Michel et al.* [1995] and *Bhandari et al.* [1993] to calculate cosmogenic nuclide production rates in stony meteorites.

2.2. Nuclear Reactions Simulation

Our model for the simulation of the interactions of primary and secondary cosmic ray particles with matter is based on the GEANT [*Brun et al.*, 1987] and MCNP [*Briesmeister* 1993] code systems. These codes were designed to simulate by Monte Carlo techniques in a very general way all the relevant physical processes taking place by the interaction of particles with nuclei. The incident primary cosmic ray particles are transported through matter considering atomic (e.g., ionization energy losses) and nuclear (elastic and inelastic) interactions. In nuclear interactions, new particles emerge that are subsequently transported and induce further interactions. GEANT is used for the simulation of transport and interactions of all charged particles (protons, alpha particles, electrons, pions, muons, etc.) and neutrons with energies above 20 MeV. The complete information about neutrons below 20 MeV (coordinates and kinematical parameters) is stored in a special file, which serves as an input file for the MCNP code. This code was designed to simulate transport and interactions of such neutrons. The main difference between these two codes consists in parameters (like cross sections) used for simulations. GEANT models particle-nucleus interactions using global parameters designed for all nuclei, while MCNP uses a library of evaluated detailed cross sections in this energy region, where resonant structure plays an important role. These cross sections were taken from ENDF/B-VI for each neutron reaction considered in our simulation.

In previous calculations [*Masarik and Reedy, 1995*] we used the combination of LCS and MCNP codes for simulation of nuclear processes involved in cosmogenic nuclide production. The transition from LCS to GEANT was dictated by the built-in physics of these codes. This model is applicable only for particles with energies of a few GeV, and with some approximations to 10 GeV. Because of the deflection of low-energy cosmic ray particles by the geomagnetic field, only particles with energies above 10 GeV are allowed to penetrate into the atmosphere at low latitudes. GEANT was written for particle physics and is well suited to study the cosmic ray interactions in the atmosphere.

The features of high-energy particle interactions with matter are to a certain extent determined by their type and energy. In our simulations, primary particles with energies between 10 MeV and 1000 GeV were considered. The characteristic feature of the particle interactions at these energies is the production of secondary particles. Many of those secondary particles have enough energy to initiate further inelastic interactions, which produce a next generation of secondary particles. In thick targets, this leads to the generation of an internuclear particle cascade. As cosmic rays consist mainly of strongly interacting protons and alpha particles, the so-called hadronic cascade (composed of interacting particles) is produced. The hadronic cascade is usually accompanied by an electromagnetic cascade (composed of electrons, positrons, muons, photons, and neutrinos), which becomes important in the production of cosmogenic nuclides mainly by muons only at great depths below the Earth's surface.

Another type of cascade considered in the simulations is the intranuclear cascade. The intranuclear cascade model is the most frequently used approximation of high-energy hadron-nucleus interactions employed in computer simulations. The basic assumption of this model is that at high energies the interaction of the incoming hadron with the target nucleus can be considered as a nucleon-nucleon process. All the reaction products of such collisions are assumed to behave in the same way until all have left the nucleus, participating in the development of the above-mentioned intranuclear cascades, or until the particle energies become too low for further interactions. After the cascade phase of interaction the nucleus is usually still excited, and some additional particles can be emitted from the nucleus during the preequilibrium and evaporation (equilibrium) phases of the interaction.

Our model uses only basic particle and nuclear data to simulate particle interactions with matter. The energy and direction of the primary particles are selected from a specified distribution (described in the next section) using random numbers. The coordinates of an inelastic interaction of a primary particle are randomly selected considering both ionization energy losses along its trajectory and cross sections for the various possible reactions with the target nuclei. If such an interaction takes place, first an intranuclear cascade of the particle within the target nucleus is simulated. After a pre-equilibrium simulation, the nucleus is then completely de-excited using an evaporation model. All the emitted particles are subsequently followed until they are absorbed by nuclei, are completely stopped, or have escaped from the atmosphere. The produced particles are recorded together with their energies to get their differential fluxes as a function of atmospheric depth and geomagnetic latitude. A sufficient number of primary particle interactions is simulated to calculate particle fluxes with statistical errors below 5%.

2.3 The Physics Modules of Simulation Packages

The main part of the high-energy simulations is based on High Energy Transport Code (HETC) [Armstrong and Chandler, 1972]. The collision model in HETC is Intra-Nuclear Cascade Evaporation (INCE). The INCE model is applicable only for energies of a few GeV. At higher energies, a scaling model with automatic parameter update for nonelastic collisions is used. For the energies above 10 GeV, that are also of interest for this work, a multichain fragmentation model of hadron-nucleus collisions was developed. We used its realization in the form of the Monte Carlo code FLUKA [*Arnoi et al.*, 1986]. Primary particles are scattered on small angles by multiple Coulomb scattering. For all charged particles, ionization energy losses are considered.

As all the details of the basic codes are described in references above, we concentrate here only on their

extensions that are important for the present applications. Elastic scattering is usually not taken into account in the basic HETC calculations. In the codes used here, this process was considered. Elastic cross sections for neutrons were adopted from the HILO library [*Alsmiller Jr. and Barish*, 1981] in the energy range from 15 to 1500 MeV, and values from the NASA library [*Wilson and Costner*, 1975] were used for neutrons above 150 MeV. For protons, cross sections from the NASA library are used above 100 MeV and elastic scattering is neglected at lower energies. Approximate expressions based on the optical model A-THREE *[Auerbach,* 1978] were used for the scattered distributions. It should be noted that these simple formulae are needed only for predicting the shape of the angular distribution. The absolute magnitude of the differential scattering cross sections is not needed for the Monte Carlo selections, as the normalization is provided by the value of elastic cross sections taken from the tables. Comparison of approximations with the experimental data that are very rare above 150 MeV shows a good agreement within a few percent. In the evaporation calculations, the latest evaluated atomic masses are used in determining binding energies. For nuclides with masses outside of the range of the input data the masses are calculated using the Cameron semi empirical mass formula [*Cameron,* 1957].

Another important parameter in the evaporation model is the density of nuclear energy levels. This parameter is sensitive to the shell structure of the nucleus. However, a constant value of the parameter $B_0 = 8$ gives fairly good approximations for the elements present in the atmosphere. The emitted evaporated particles are not distributed isotropicaly. This is because of the nonzero angular momenta of excited nuclei and mainly by their recoil energy that is included in the simulation procedure [*Prael and Lichtenstein,*1989]. The competitive process to the evaporation of light particles is high-energy fission, which is built into our simulation package in the form of the RAL model *[Atchison,* 1980]. Neutral pions have a very short half-life and are considered to decay at the collision site where they are created. Photon fluxes from their decays are calculated, taking into account the g-g and the Dalitz-decay channels. For charged pions in flight (before coming to rest because of ionization energy losses) both decay and nuclear collisions are taken into account. Positive pions that come to rest are assumed to decay or undergo nuclear capture. If the negative pion becomes captured when stopped, the capture products are computed using the INC model with the initial value of energy corresponding to the rest mass energy. All the simulations are done in combinatorial complex geometry and in three dimensions. The complete information about the particles stored in the auxiliary files enables us to calculate particle fluxes, currents, and production probabilities as function of space coordinates. The details of the normalization of our results to the galactic cosmic ray particle flux are given in section 3.1.

2.4. Geometrical and Chemical Model of the Earth

In our calculations the solid Earth was considered as a sphere with a radius of 6378 km, a surface density of 2 g cm^{-2} [illegible] Table 1. The Earth's atmosphere was modeled as a spherical shell with an inner radius of 6378 km and a thickness of 100 km. The atmospheric shell was divided into 34 concentric subshells of equal thickness (g cm^{-2}) with the average chemical composition given in Table 1. The thickness of a shell was chosen as a compromise between two opposite requirements: minimization of statistical errors, which are approximately inversely proportional to the shell thickness, and resolution of the depth dependence of particle fluxes, which increases with the number of shells. Each shell was divided into 9 latitudinal sections corresponding to steps of 10 degrees in magnetic latitude. The atmospheric density was approximated by $\rho = 1.27 \times 10^{-3}\, e^{-0.1091\, h}$ g cm^{-3} for $h < 9.73$ km and $\rho = 2.03 \times 10^{-3}\, e^{-0.1573\, h}$ g cm^{-3} for $h > 9.73$ km, where h is the altitude above sea level in km. The temperature structure of the atmosphere was in accordance with the U.S. Standard Atmosphere, 1976, model [*Champion et al.,* 1985].

Table 1. Elemental Composition (in Weight Fraction) Adopted for These Calculations

Element	Soil	Atmosphere
H	0.002	
N		0.755
O	0.473	0.232
Na	0.025	
Mg	0.040	
Al	0.060	
Si	0.290	
Ar		0.013
Ca	0.050	
Fe	0.060	

The simulation of 5,000,000 primary protons for each latitudinal section lead to statistical errors of 4-5% for neutrons near the Earth's surface and 3-4% in the upper atmosphere. Statistical errors of the proton fluxes were on the level of 4-5% in the stratosphere and were above 10% at larger depths. However, since the proton fluxes are more than *1* order of magnitude smaller than the neutron fluxes, their uncertainties are not significant for the final results. The errors resulting from the assumed average composition of the atmosphere and surface are also not significant because it was found in earlier simulations [*Masarik and Reedy,* 1994] that, except for hydrogen, small changes in the abundance of the elements affect only a little the calculated particle fluxes. The systematic uncertainties in our calculated fluxes are difficult to determine, but are probably on the order of 10%.

2.5. Cosmic Ray Particle Fluxes

The simulation of particle production and transport processes begins with the choice of the primary particle type and its energy. The primary cosmic ray flux at the Earth's orbit has two components: galactic cosmic rays (GCR) and solar cosmic rays (SCR).

The GCR particles are a mixture of ~87% protons, ~12% alpha particles and ~ 1% of heavier nuclei with atomic numbers from 3 to ~ 90 [*Simpson,* 1983]. The spectral distributions of all particles look quite similar if [illegible]

propagation of the GCR particles to the Earth is influenced by many interactions that lead to spatial and temporal variations. The dominant effect is the solar modulation, which is taken into account in the expression for the differential primary GCR proton flux. In our calculations we used the *Castagnoli and Lal* [1980] formula for the differential spectra of GCR primary protons:

$$J(E_p,\Phi) = C_p \frac{E_p(E_p+2m_pc^2)(E_p+x+\Phi)^{-2.5}}{(E_p+\Phi)(E_p+2m_pc^2+\Phi)} \quad (2)$$

where $x = 780 \exp(-2.5 \times 10^{-4} E_p)$, E_p is the proton's kinetic energy, φ is the parameter that takes into account the modulation effect due to solar activity, m_p is the mass of the proton, c is the velocity of light, m_pc^2 is 938 MeV, and $C_p = 1.244 \times 10^6$ cm $^{-2}$s^{-1}MeV^{-1} is the normalization factor. For GCR alpha particles and heavier nuclei, analogous formulae hold with slightly different parameters [*Lal,* 1988]. Since differences in cross sections for neutron and proton emission in reactions of primary GCR protons and alpha particles are very small, we simulated only the homogeneous and isotropic irradiation of Earth with primary protons. From the fitting of lunar experimental data [*Reedy and Masarik,* 1994], the effective flux of protons with energies above 10 MeV at 1 AU was determined to be 4.56 nucleons cm^{-2}s^{-1}. This value corresponds to the modulation parameter φ = 550 MeV, which is identical to the long-term average value [*Reedy,* 1987]. To study the influence of solar modulation, we carried out detailed simulations for modulation parameters varying from 0 to 1000 MeV that cover the whole range of modulation parameters observed in the past.

The solar cosmic rays consist of ~98% protons and ~2% heavier nuclei. The energies are typically in the range 1 - 100 MeV. Because of their relatively low energies, they can cause nuclear reactions in the Earth's atmosphere only at high geomagnetic latitudes (above 60°), and even there the nuclide production is restricted to the very top of the atmosphere. The long-term average production of cosmogenic nuclides by SCR is not expected to be significant. Some huge solar particle events produce proton fluxes much higher than the average [*Shea and Smart,* 1992], and they could make a contribution to some cosmogenic nuclide production (e.g., ^{7}Be and ^{36}Cl) observable in some layers in polar ice, such as from Greenland and Antarctica. Calculations confirming these expectations with the analysis of obtained results were published earlier [*Masarik and Reedy,* 1995].

2.6. The Geomagnetic Field

The geomagnetic field of the Earth deflects incoming cosmic ray particles depending on their magnetic rigidity and angle of incidence. The rigidity of a particle is defined as the momentum per unit charge, $R = pc/Ze$, where p is the momentum, Ze is the charge of the particle, and c is the velocity of light. The vertical cutoff rigidities used in the calculations are shown in Figure 1 [*Shea and Smart,* 1983] The nonvertical cutoff rigidities were calculated with the aid of the computer code *ANGRI* [*Bland and Cioni,* 1968]. Using the relativistic equation for energy-momentum, the cutoff energy can be calculated and all particles with lower energies are excluded from the simulations. In order to investigate the influence of geomagnetic field variations on particle fluxes and cosmogenic nuclide production rates, the relative intensity of the geomagnetic field was varied from 0 to 2, relative to the present field in steps of 0.25. The shape of the field was left unchanged.

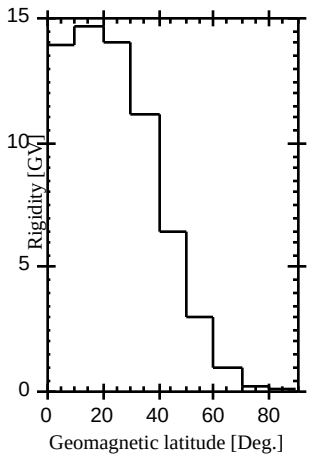

Figure 1. Vertical cutoff rigidities as a function of geographical latitude.

2.7. Cross Sections for Cosmogenic Nuclide Production

The main target elements in the atmosphere are nitrogen, oxygen, and argon. For reactions on oxygen, the same cross sections were used as in the case of extraterrestrial material [*Masarik and Reedy,* 1994*; Reedy and Masarik,* 1994*; Reedy et al.,* 1993]. For nuclear reactions on nitrogen and argon, experimental cross sections were used whenever possible. Otherwise they were estimated from similar reactions on other isotopes. For the tritium production the cross sections of *Nir et al.* [1966] were applied.

For the N(p,x)^{7}Be and N(p,x)^{10}Be reactions, experimental cross sections were used *[Bodemann et al.,* 1993*; Reyss et al.,* 1981*; Raisbeck and Yiou,* 1976*; Michel et al.,* 1995b*; Michel et al.,* 1997*; Schiekel et al.,* 1996a]. The cross sections for the reaction N(n,x)^{7}Be reactions were identical with those for the (p,x) reaction above 300 MeV but decreased rapidly to zero at a neutron energy of 42 MeV. The cross sections for the N(n,x)^{10}Be are those for (p,x) reactions above 600 MeV and measured values for neutrons with energies below 35 MeV [*Nakamura et al.,* 1992].

Measured cross sections were used for the Ar(p,x)^{36}Cl reaction [*Huggle at al.,* 1996*; Parrat et al.,*1996*; Schiekel et al.,* 1996b]. Below 40 MeV, ^{40}Ar(p,αn)^{36}Cl is the main reaction with a threshold of only 7.2 MeV. Except for the threshold at 40 MeV, the same cross sections were taken for the reaction ^{40}Ar(n,$p4n$)^{36}Cl above 80 MeV. Cross sections for the ^{36}Ar(n,p)^{36}Cl

reaction were calculated using the LAHET code system.

As an example for cross sections used in our calculations, we present in Figure 2 experimental cross sections for the production of ^{10}Be from nitrogen and oxygen. Cross section values between the experimental data points were obtained by linear interpolation. For values with energies above the presented range, cross sections equal to the highest experimental data point were taken. The same procedure was applied to construct the excitation functions for the other nuclear reactions.

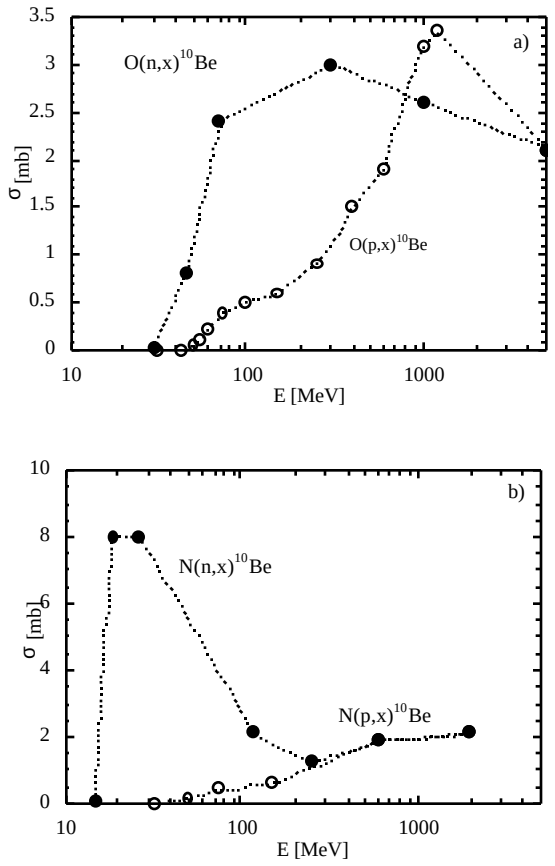

Figure 2. Cross sections for the production of ^{10}Be from (a) O and (b) N used in the calculations. See text for references to experimental data.

With the development of AMS the production rates of some other nuclides, like ^{26}Al, ^{22}Na, and ^{32}Si also were measured. We did not calculate their production rates, because there are no reliable cross sections available for them. Our calculated particle fluxes are accessible on the Web and can be used to calculate the production of any radionuclide, provided the corresponding cross sections are available.

The uncertainties of the cross sections for nitrogen and argon are difficult to estimate, because they have not been tested in extraterrestrial materials. The uncertainties of proton cross sections are probably within their measuring errors, which are usually below 10% for the latest data and 20% or even more for older data. The uncertainties in evaluated cross sections for neutron-induced reactions are unknown, but probably less than 50%. The reported uncertainties for the measured neutron cross sections are on the level of 25%. The lack of precise cross sections for the production of different nuclei from the target elements of interest represents the largest contribution to the uncertainty of these calculations.

3. Results and Discussion

3.1. Particle Fluxes in the Atmosphere.

Figure 3 shows the depth dependence of the integral proton and neutron fluxes in the Earth's atmosphere for the solar modulation parameter φ = 550 MeV. The neutron flux is larger by almost 2 orders of magnitude. Note that the neutron flux reaches its maximum in the depth interval 75 - 125 g cm^{-2}. This maximum is present at all latitudes and originates from the development of the particle cascade and the depletion of the neutron density at high altitudes by neutron leakage out of the atmosphere. At atmospheric depths exceeding ~180 g cm^{-2}, the total flux shows an exponential decrease with an effective attenuation length between 150 g cm^{-2} near the poles and 172 g cm^{-2} near the equator (Figure 3). This exponential dependence is disturbed only near the bottom of the atmosphere, where the total neutron flux shows considerable variations as was already discussed by *O'Brien et al.* [1978] and *Masarik and Reedy* [1995]. The latitude dependence of the incident primary cosmic ray flux is reflected in the total neutron flux. However, the effect is somewhat smaller than for the proton flux because of the logarithmic dependence of the neutron multiplicity on energy. The principal feature of the depth dependence of the total proton flux is a strong decrease with increasing depth in the atmosphere. However, the decrease is weaker at lower latitudes where the primary input spectrum is harder.

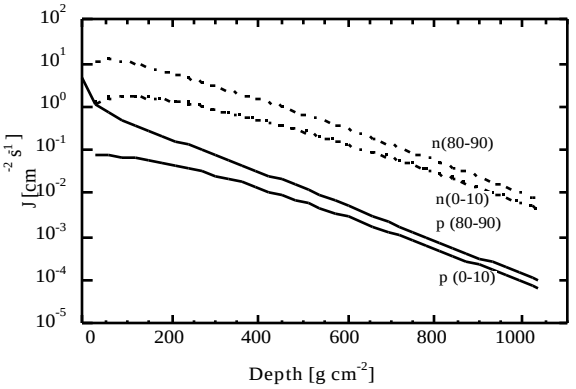

Figure 3. Integral proton and neutron fluxes (E > 1 MeV) in the Earth's atmosphere for the solar modulation parameter φ= 550 MeV, latitude 0° - 10° and 80° - 90°.

In order to analyze production rates of cosmogenic nuclides in the atmosphere as a function of altitude, latitude, and other parameters, we calculated the depth-dependent differential energy spectra of protons and neutrons (Figure 4). All differential proton fluxes show broad maxima, the location of which are energy dependent, and a gradual decrease toward lower energies caused by the increasing influence of the Coulomb interaction. At shallow depths, the maximum is shifted to higher energies because of the contribution from primary

cosmic ray particles, which have their maximum around 1 GeV. The exclusion of the low-energy protons (with rigidities below cutoff rigidity) from the input primary cosmic ray spectrum for low latitudes explains the observed differences in proton spectra near the top of the atmosphere for low and high latitudes. Protons are prevailing particles for energies above 800 MeV near the top of the atmosphere. Below this energy, neutrons are the dominant particle type by orders of magnitude. The neutron spectra show an exponential decrease with increasing energy, which is somewhat disturbed near the top of the atmosphere because of leakage, as mentioned above. For depths greater than ~150 g cm^{-2}, the equilibrium in the production and attenuation of the particles is reached and the shape of the neutron energy spectrum varies only very slowly with the depth. The relative contribution of neutrons to the total flux of cosmic ray particles increases from 90% near the top of the atmosphere (30 g cm^{-2}) to 98% at sea level. Because the production yield of cosmogenic isotopes peaks in the low-energy region, the overwhelming majority of cosmogenic nuclides are produced by neutron reactions.

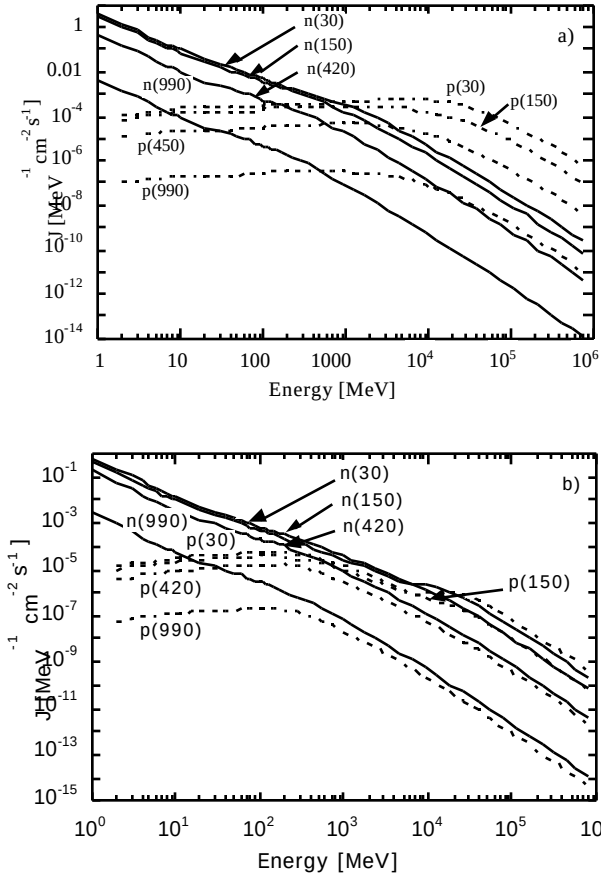

Figure 4. Differential neutron and proton fluxes in the Earth's atmosphere for the solar modulation parameter φ = 550 MeV, for four depths (30, 150, 420 and 990 g cm^{-2}) and for latitudes (a) 80° - 90°.and (b) 0° - 10°.

The spectra of muons and pions were also calculated; however, they are not important for the production of cosmogenic nuclides in the atmosphere and are not discussed here. The exclusion of the muons from the calculation of cosmogenic nuclide production is based on the fact that they participate only in the weak and electromagnetic interactions and therefore induce only a few nuclear reactions. Though the pions interact strongly, they are omitted in the final cosmogenic nuclide calculations because there are 100 to 1000 times less pions than protons in the Earth's atmosphere.

Our calculated particle fluxes were compared with accessible experimental data from neutron monitors. The comparison is based on the fact that the count rate of a neutron monitor is proportional to the intensity of the nucleonic component (in the equilibrium region of the atmosphere). Latitude and altitude dependencies of neutron and proton fluxes were compared with data presented in Table II of *Carmichael and Bercovitch* [1969]. The results of the comparison are presented in Table 2 here. A good agreement between experimental and calculated data was found.

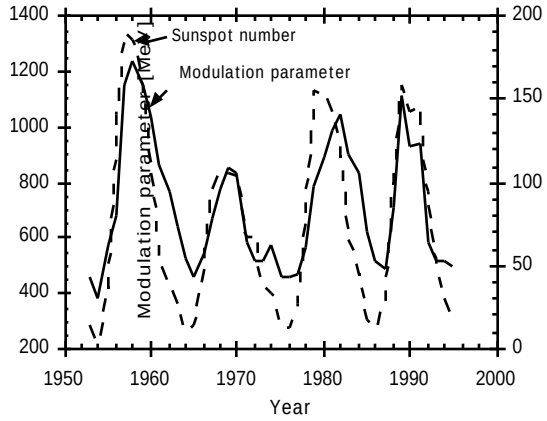

Figure 5. Solar modulation parameters φ for the period 1953-1995 determined from Deep River neutron monitor data and our calculations along with the mean annual Wolf sunspot numbers.

The solar modulation of GCR is expressed in our primary cosmic ray spectrum through the modulation parameter φ. *Neher* [1967] measured the cosmic ray proton spectrum during a series of balloon flights in July and August 1965. The resulting proton spectrum, in the energy range from 50 MeV to 12 GeV, is best fitted with the modulation parameter φ = 450 MeV. Then we calculated nucleon fluxes at the Deep River neutron monitor site for various modulation parameters and its detection efficiency. Using a value of φ = 450 MeV and the neutron monitor efficiency, the calculated nucleon flux was converted into the neutron monitor counting rate for this time period. In the inversion procedure, we used the relative contributions of neutrons and protons to the counting rate of the neutron monitor determined by *Hughes and Marsden* [1966]. Within the statistical errors of calculations, the calculated and experimental counting rates agree. From the comparison of the Deep River neutron monitor counting rate and our calculated nucleon flux at this location, the solar modulation parameter was determined for the years 1953-1995.The determined values of φ during the investigated time

Table 2. Comparison of Experimental [*Carmichael and Bercovitch*, 1969] and Calculated Latitude Variation of Nucleon Fluxes in the Earth's Atmosphere for Three Different Depths (Altitudes in the Atmosphere Above Sea Level

Vertical Cutoff, GV	1033 g cm^{-2} [0 km] n-monitor, %*	1033 g cm^{-2} [0 km] calculated, %*	843 g cm^{-2} [1.68 km] n-monitor, %*	843 g cm^{-2} [1.68 km] calculated, %*	680 g cm^{-2} [3.4 km] n-monitor, %*	680 g cm^{-2} [3.4 km] calculated, %*
1	100.0	100.0	100.0	100.0	100.0	100.0
2	99.3	99.4	99.3	99.3	99.4	99.3
2.5	98.1	98.6	97.7	97..8	97.5	97.4
3	96.5	97.5	95.7	96.2	94.9	94.7
3.5	94.7	95.7	93.1	93.6	91.9	92.8
4	92.8	94.7	90.4	91.3	88.6	89.5
5	88.8	91.5	85.1	86.0	82.2	83.9
6	84.7	88.2	79.8	80.6	76.3	77.9
7	80.5	84.3	74.8	76.3	70.6	72.0
8	76.5	81.4	70.0	72.2	65.4	67.4
9	72.6	77.2	65.5	68.2	60.5	63.0
10	68.9	73.3	61.3	64.2	56.1	58.4
11	65.4	70.3	57.5	61.2	52.2	54.9
12	62.1	66.8	53.9	57.3	48.4	51.5
13	59.3	64.1	50.8	54.4	45.2	48.1
14	56.7	61.6				

* Percentage of high-latitude value.

Table 3. Latitudinal and Global Average Production Rates (Atoms cm^{-2} s^{-1}) in the Earth's Atmosphere for Long Term Mean Solar Activity (φ = 550 MeV) and Present Geomagnetic Field Intensity.

Nuclide	Latitude Deg. 0-10	10-20	20-30	30-40	40-50	50-60	60-90	Global Average#
^{3}H	0.118	0.129	0.159	0.224	0.380	0.565	0.602	0.281
^{7}Be	0.0148	0.0161	0.0197	0.0285	0.0478	0.071	0.0740	0.0354
^{10}Be	0.00775	0.00841	0.0104	0.0147	0.0248	0.0368	0.0386	0.0184
^{14}C	0.83	0.90	1.10	1.56	2.63	3.92	4.55	2.02
^{36}Cl	7.91e-4	8.60e-4	1.05e-3	1.51e-3	2.52e-3	3.75e-3	3.96e-3	0.00188

period are given in Figure 5, along with the annual Wolf mean sunspot numbers. The obtained range is somewhat larger than the one presented by *Reedy* [1987], but smaller than that of *Lal* [1988]. In general accord with solar activity, there is an approximate inverse correlation between solar activity and cosmic ray flux, but the data does not show a one-to-one correlation.

The calculated fluxes, together with software necessary for the calculation of cosmogenic nuclide production rates are on the internet at www.eawag.ch/~masarik.

3.2 Production Rates of Cosmogenic Nuclides

Using the calculated particle fluxes in the atmosphere, the production rates of ^{3}H, ^{7}Be, ^{10}Be, ^{14}C, and ^{36}Cl were determined. The latitudinally and globally averaged production rates for the modulation parameter φ = 550 MeV, which was derived from lunar and meteoritic samples as the long-term mean value, are in Table 3.

The best investigated cosmogenic nuclide in the Earth's atmosphere is ^{14}C. Because many theoretical models and experimental procedures were developed for the determination of its production rate, it seems justified to provide more details about the calculations of its production rate. On the basis of previous work [*Masarik and Reedy*, 1995], we considered in our simulations only the nuclear reaction ^{14}N(n,p)^{14}C. This reaction with its more than 99% contribution to the total production rate of ^{14}C is by far the most important source of ^{14}C in the atmosphere. We calculated a mean production rate of 1.96 $\times 10^{-3}$ ^{14}C atoms g^{-1} s^{-1} in the Earth's atmosphere. Integrating over the depth of the atmosphere, a global average production rate of 2.02 ^{14}C atoms cm^{-2} s^{-1} is obtained. Its uncertainty of ~10% is mainly due to uncertainties and statistical errors in the neutron fluxes (the cross sections are well measured). This new value is about 5.7% higher than the one in *Masarik and Reedy* [1995]. The reason for the difference is the improvement in the simulations of production and transport of neutrons at low latitudes. It is in good agreement with estimates of the radiocarbon production rate based on the analysis of the specific activity of ^{14}C (e.g., 1.99 atoms cm^{-2} s^{-1} [*Damon et al.*, 1978]) and with other theoretical models (e.g., 1.8 [*Lal and Peters*, 1967], 1.75 [*O'Brien*, 1979], and 2.01 [*Ma*

sarik and Reedy, 1995]).

The rest of the radionuclides calculated with our model and presented in the Table 3 are produced in spallogenic nuclear reactions. The uncertainties in our calculated values for these nuclides are higher than for ^{14}C, mainly because of greater uncertainties in the corresponding excitation functions. The average errors are estimated to be within 30-50%. The lack of accurate cross sections is one of the reasons of differences in their production rates obtained with various models employing various sets of cross sections. The situation is also not much better with their experimental determination. When comparing our calculated production rates with the ones derived from measurements in various environmental systems, one has to keep in mind that our calculations represent global mean values, whereas the measured data reflect to some extent local values.

Our calculated production rate for ^{10}Be of 0.0184 atoms cm^{-2} s^{-1} is close to the value measured in the Dye 3 ice core, 0.016 atoms cm^{-2} s^{-1} [*Beer et al.,* 1994], and also to the value obtained from sediment cores, 0.026 atoms cm^{-2} s^{-1} [*Reyss et al.,* 1981], but is approximately 2 times lower than that determined from ^{10}Be measurements in precipitation, 0.038 ± 0.008 atoms cm^{-2} s^{-1} [*Monaghan et al.,* 1985]. Other model estimates gave 0.045 atoms cm^{-2} s^{-1} [*Lal and Peters,* 1967], 0.014 atoms cm^{-2} s^{-1} [*Oeschger et al.,* 1969], 0.026 atoms cm^{-2} s^{-1} [*O'Brien,* 1979], 0.0201 atoms cm^{-2} s^{-1} [*Masarik and Reedy,* 1995], and the value closest to our estimate, 0.020 atoms cm^{-2} s^{-1} [*Reyss et al.,* 1981]. Our value for the ^{7}Be production rate, 0.035 atoms cm^{-2} s^{-1}, is about 2 times higher than 0.0185 cm^{-2} s^{-1} estimated by *Oeschger et al.* [1969] and about 3 times higher than 0.0129 atoms $cm^{-2}s^{-1}$ obtained by *Masarik and Reedy* [1995], but is approximately 2 times lower than the 0.0810 atoms cm^{-2} s^{-1} of *Lal and Peters* [1967] and 0.0578 calculated by *O'Brien* [1979]. Our production rate of ^{36}Cl, 1.88×10^{-3} atoms cm^{-2} s^{-1}, is in good agreement with 2.2×10^{-3} atoms $cm^{-2}s^{-1}$ of *Oeschger et al.* [1969] but is substantially higher than the 1.1×10^{-3} atoms cm^{-2} s^{-1} of *Lal and Peters* [1967], the 1.18×10^{-3} atoms cm^{-2} s^{-1} of *Masarik and Reedy* [1995], and the 9.01×10^{-4} atoms cm^{-2} s^{-1} of *O'Brien* [1979]. Our calculated production rate for ^{3}H of 0.28 atoms cm^{-2} s^{-1} agrees fairly well with 0.19 atoms cm^{-2} s^{-1} calculated by *Nir at al.* [1966], 0.26 atoms cm^{-2} s^{-1} obtained by *Masarik and Reedy* [1995], and 0.255 atoms cm^{-2} s^{-1} by *O'Brien et al.* [1978]. The reasons for the large differences between these calculations and those of *Masarik and Reedy* [1995] for ^{7}Be and ^{36}Cl were: the use of new cross sections for both radionuclides and the application of the correct value of target elements concentration (*Masarik and Reedy* [1995] took the volume fraction of argon in the atmosphere instead of the weight fraction).

Ratios of radionuclides were measured in some samples. These ratios can be influenced by transport and deposition processes, and therefore it is still under discussion how well they represent ordinary production rate ratios. The calculated production ratios for $^{10}Be/^{7}Be$, $^{7}Be/^{36}Cl$, and $^{10}Be/^{36}Cl$ are 0.52, 18.8, and 9.8, respectively. Our global $^{10}Be/^{7}Be$ ratio, which is of interest to study atmospheric transport processes, is very close to the estimated production ratio of about 0.5 [*Raisbeck et al.*, 1981]. The experimental value for the $^{10}Be/^{36}Cl$ ratio measured in samples from the Camp Century ice core in Greenland is about 8 [*Conrad et al.,* 1989], and in the Greenland Ice Core Project (GRIP) ice core it varies between 3 and 9, with the average value for the Holocene being 5.7 [*Yiou et al.,* 1997]. This ratio and the $^{7}Be/^{36}Cl$ ratio in precipitation scatter around 10 [*Knies et al.,* 1994].

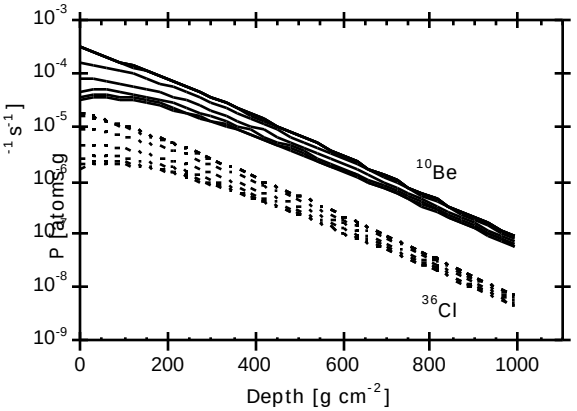

Figure 6. Depth dependent latitudinal production rates of ^{36}Cl and ^{10}Be in the Earth's atmosphere. Each line represents a latitude interval of 10°. For both nuclides, the production rates decrease with decreasing latitude for all depths in the atmosphere

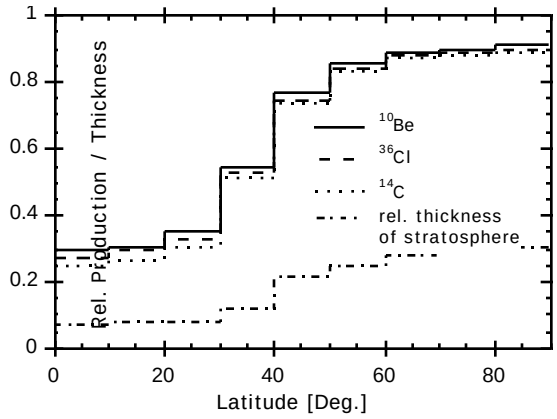

Figure 7. Relative contribution of the ^{36}Cl, ^{19}Be, and ^{14}C production in the stratosphere to the total atmospheric production and relative thickness of the stratosphere (thickness of the stratosphere divided by the total thickness of the atmosphere) as a function of latitude.

The depth dependence of the production rates for ^{36}Cl and ^{10}Be is given in Figure 6. Using these dependencies and accounting for the variation of the stratospheric thickness with latitude, Figure 7 displays the relative contribution of the stratosphere to the total atmospheric production. In the average, the stratosphere contributes 55.7%, 53.9%, 51.4%, 53.5%, and 55.1% to the production of ^{10}Be, ^{36}Cl, ^{14}C, ^{7}Be, and ^{3}H, respectively. The relative contribution of the stratosphere to the average global production rate of ^{14}C is in good agreement with the 56% determined by *Lal and Peters* [1967] and the 61% calculated by *O'Brien* [1979]. The differences for spallation products are probably greater but cannot be compared directly, because in both former papers, only the production rates of stars (inelastic

stratosphere is produced 66 and 79 % of all stars, according to Lal and Peters [1967] and *O'Brien* [1979], respectively.

The latitudinal production rates as a function of the solar modulation parameter φ are presented in Figure 8 for the present geomagnetic field intensity. As a consequence of the lower magnetic cut off rigidity, the solar modulation effect is maximal at high latitudes. The ratios of the calculated ^{10}Be production rates between the latitudinal bands 80°-90°and 0°-10° are 8.7 and 3.7 for the solar modulation parameters 0 and 1000 MeV, respectively. The corresponding ratios are 9.8 and 4.1 for ^{14}C and 8.9 and 3.7 for ^{36}Cl. These ratios are consistent with the fact that the relative contribution of high-energy particles is highest for the ^{10}Be production, and therefore the ^{10}Be ratio is smallest. The largest variation is obtained for ^{14}C, which is produced by thermal and epithermal neutrons.

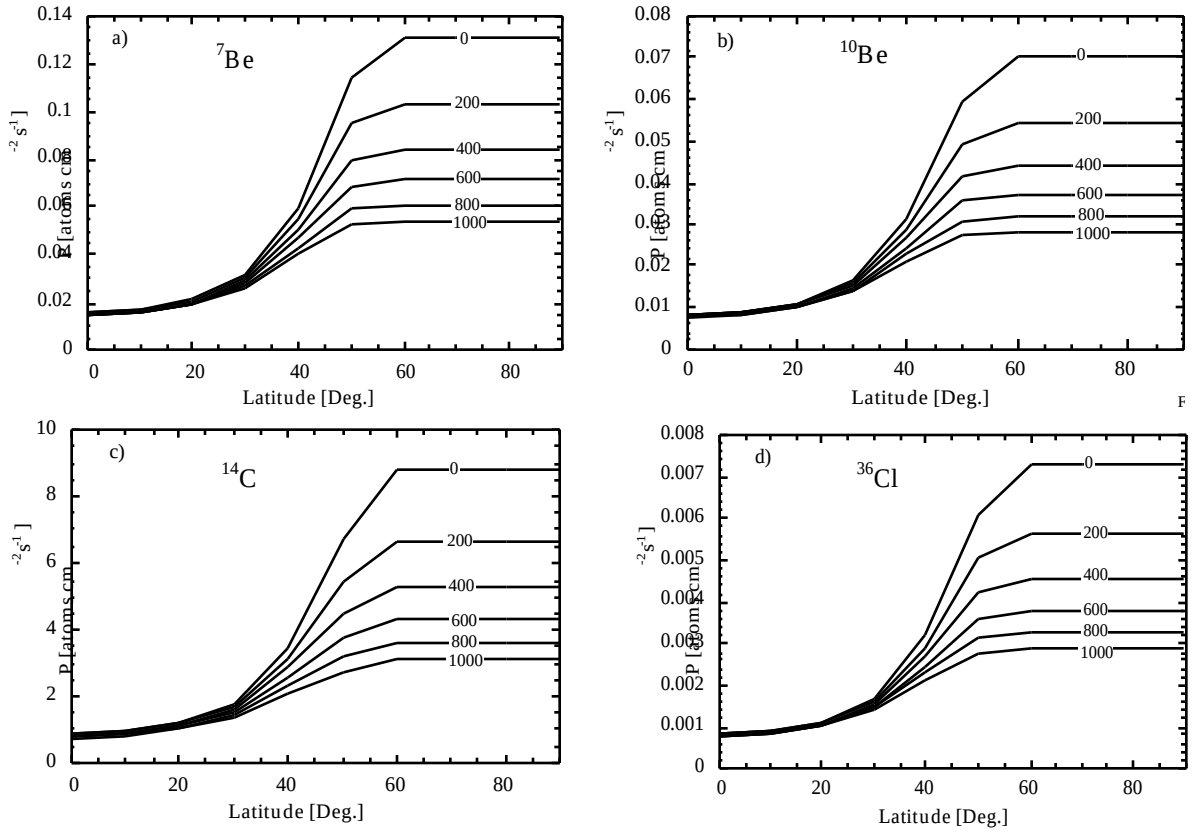

Figure 8. Depth integrated latitudinal production rates of (a) ^{7}Be, (b) ^{10}Be, (c) ^{14}C, and (d) ^{36}Cl in the Earth's atmosphere for the solar modulation parameter φ = 0, 200, 400, 600, 800, and 1000 MeV.

The dependencies of the latitudinal production rates and global average production rate for the investigated nuclides on the solar modulation parameter are presented in Figure 9. They clearly show that solar modulation for latitudes below 30° is small. For the latitudinal band 0°-10° the production ratios between modulation parameter 0 and 1000 MeV is 1.07, 1.07, and 1.18 for ^{10}Be, ^{36}Cl, and ^{14}C, respectively. The solar modulation effect is most pronounced for high latitudes where the corresponding ratios are 2.51, 2.56, and 2.81. These results can be understood within the frame of the interplay between the solar modulation and the geomagnetic field intensity. At low latitudes, the geomagnetic field reflects preferentially low-energy particles, and since the solar modulation effect on high-energy primary particles is small, the net effect is small too. In the case of high latitudes on the other hand, all primary cosmic ray particles can enter the Earth's atmosphere and interact with its atoms. Since the low-energy end of the spectrum is strongly modulated by the Sun and represents a considerable part of the total spectrum, the resulting effect is relatively large.

To estimate the production variation during a typical 11-year Schwabe cycle, we assumed that φ varies between 300 (solar minimum) and 900 MeV (solar maximum). This leads to changes of the production rates by factors of 1.34 and 1.46 for spallogenic products and ^{14}C, respectively. The global production rates for cosmogenic nuclides produced in the Earth's atmosphere by spallogenic reactions during solar minimum are about 1.15 times higher compared to the average over a complete solar cycle, and the rates at solar maximum are 0.85 times the average rates. The equivalent quantities for ^{14}C are 1.19 and 0.82.

For many geophysical applications, it is useful to know the magnitude of variations of cosmogenic nuclide production rates for a varying geomagnetic field. From sedimentary paleomagnetic records, it is known that the intensity of the geomagnetic field varied in the past from

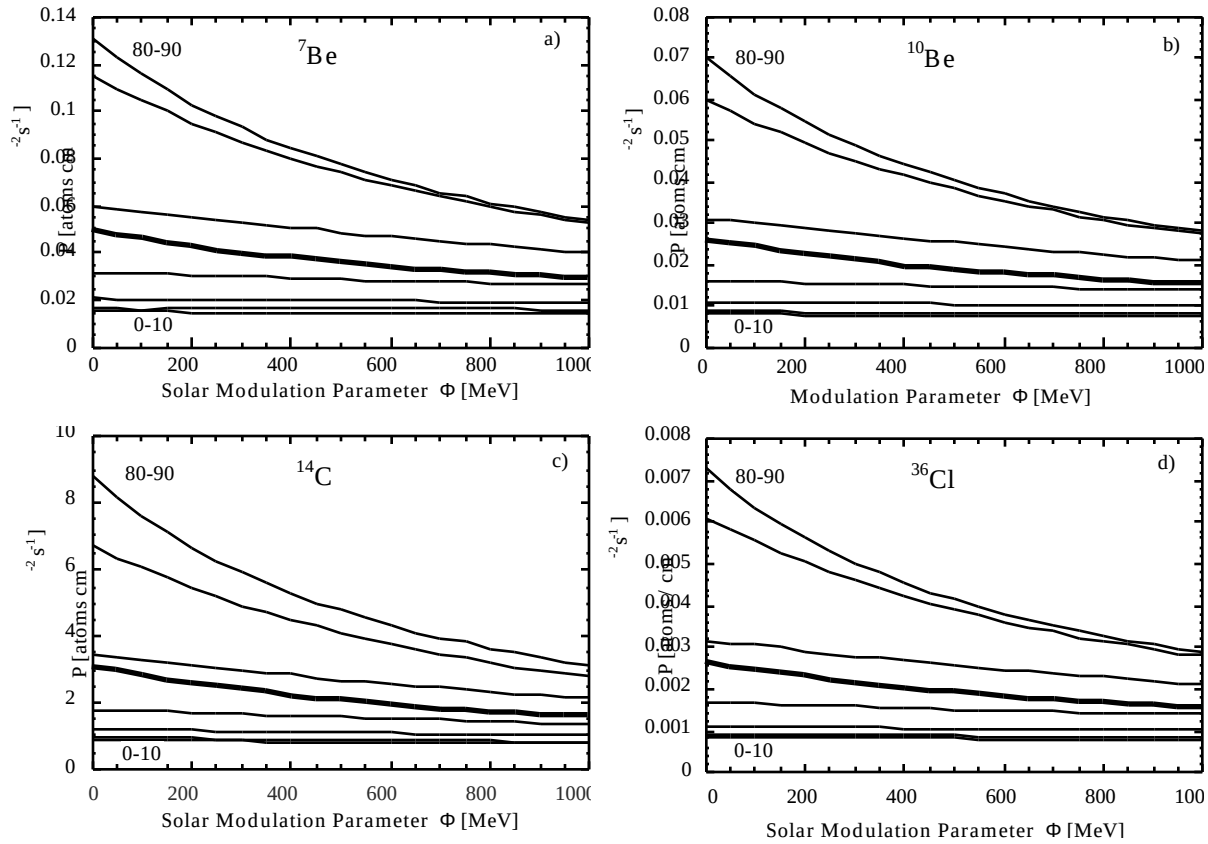

Figure 9. Dependencies of global average (thick line) and latitudinal (thin line) production rates of (a) ^{7}Be, (b) ^{10}Be, (c) ^{14}C, and (d) ^{36}Cl in the Earth's atmosphere on the solar modulation parameter. Each line represents a latitude interval of 10°. The latitudinal production rates decrease with decreasing latitude for all modulation parameters.

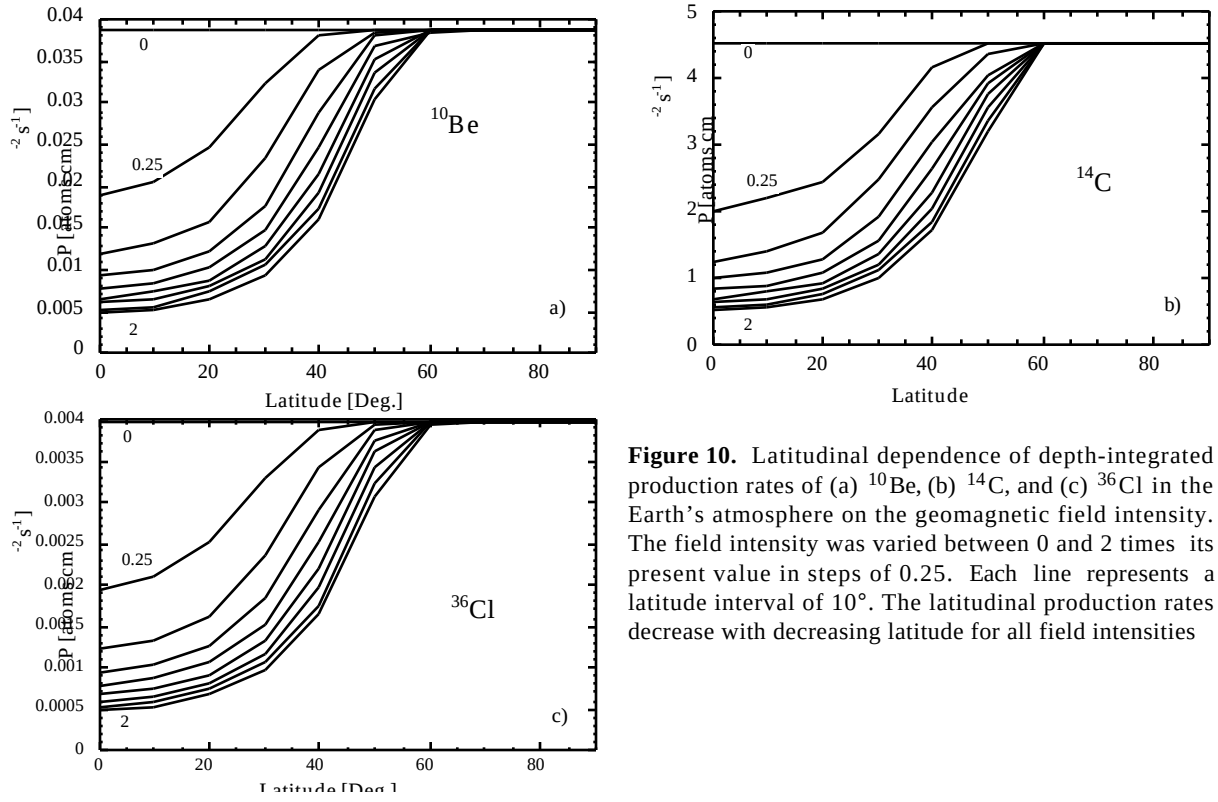

Figure 10. Latitudinal dependence of depth-integrated production rates of (a) ^{10}Be, (b) ^{14}C, and (c) ^{36}Cl in the Earth's atmosphere on the geomagnetic field intensity. The field intensity was varied between 0 and 2 times its present value in steps of 0.25. Each line represents a latitude interval of 10°. The latitudinal production rates decrease with decreasing latitude for all field intensities

almost zero to twice its present intensity [*Guyodo and Valet,* 1996]. Therefore we carried out simulations of the production rates of cosmogenic nuclides in the Earth's atmosphere for this intensity range.

The latitudinal dependencies of the production rates for long-lived radionuclides (^{10}Be, ^{36}Cl, and ^{14}C) are presented in the Figure 10, assuming a solar modulation parameter φ = 550 MeV. Equivalent dependencies were also calculated for a solar modulation parameter φ varying from 0 to 1000 MeV. They were used to calculate the average global production rates.

From the analysis of the calculated dependencies, it follows that changes in the geomagnetic field intensity lead to substantial changes in the atmospheric production rate pattern for all investigated nuclides. For example, for the solar modulation parameter φ = 550 MeV and the present geomagnetic field intensity the ratio of latitudinal production rates varies by about a factor of 8 for spallogenic products and by a factor of 9 for ^{14}C. The ratios for the global average production rate for zero geomagnetic field and a doubling of the present intensity are 2.7, 2.7, and 2.9 for ^{10}Be, ^{36}Cl, and ^{14}C, respectively. In the extreme case (zero intensity of geomagnetic field and solar modulation parameter φ = 0 to a doubling of the geomagnetic field intensity and a solar modulation parameter φ = 1000 MeV), the global average production ratios for ^{10}Be, ^{36}Cl, and ^{14}C are 5.9, 6.0, and 8.6, respectively. The above calculated dependencies were used to reconstruct the ^{36}Cl data from the Summit GRIP ice core and to estimate the contribution of geomagnetic field intensity variations to their most pronounced features, like the Laschamp event, at least 80 % of which can be explained by a decrease of the geomagnetic field [*Baumgartner et al.*, 1998]

4. Conclusions

A purely physical Monte Carlo model based on the codes GEANT and MCNP was used to simulate production and transport of galactic cosmic ray particles in the Earth's atmosphere for energies ranging from subthermal to hundreds of GeV. The model enables us to calculate differential particle fluxes as a function of geomagnetic latitude, altitude, chemical composition, geomagnetic field intensity, and solar modulation. The calculated particle fluxes are in a reasonable agreement with experimental data from neutron monitors. They have been used for the calculation of cosmogenic nuclide production rates in the Earth's atmosphere.

The calculated production rate of ^{14}C in the Earth's atmosphere is 2.02 atoms cm^{-2}s^{-1} and agrees well with experimentally determined and other calculated values. The comparison of our calculated values for ^{3}H, ^{7}Be, ^{10}Be, and ^{36}Cl is not so unique, as experimental and other calculated values differ, often substantially. The calculated ratios of investigated nuclides agree fairly well with experimental data obtained from measurements in ice cores and precipitation samples.

The dependence of the production rates on variations of the solar activity and the geomagnetic field strength was investigated in detail. The good agreement of calculations with modern measured values shows that our model can be used to obtain reliable production rates of terrestrial cosmogenic nuclides and also that our model should be good for samples from very large depths in extraterrestrial objects, including those with an atmosphere and magnetic field. These results provide the basis for a quantitative reconstruction of the history of the solar activity and the geomagnetic field intensity using records of cosmogenic isotopes in natural archives such as sediments and ice cores.

Acknowledgments. We thank many of our colleagues for their comments and encouragement, for some of the data used in this work, and for benchmarking our calculations. We especially appreciate the constructive comments by R. C. Reedy, A. Blinov, S. Ivy-Ochs, and G. Wagner that significantly improved this manuscript. We thank R. C. Reedy also for providing us with cross sections of nuclear reactions. This work was supported by the Swiss National Science Foundation.

References

Alsmiller, R.G.,Jr., and J. Barish, Neutron-photon multigroup cross sections for neutron energies < 400 MeV, ORNL/TM-7818, 76 pp., Oak Ridge Natl. Lab., Oak Ridge, Tenn., 1981.

Arnoi, P.A., A. Fasso, H.J. Moehring, J. Ranft, and G.R. Stevenson, FLUKA86 User's guide, CERN-TIS-RP/168, 64 pp., Eur. Org. for Nucl. Res., Geneva, 1986.

Armstrong, T.W., and K.C. Chandler, HETC - A high energy transport code, *Nucl. Sci. Eng. 49*, 110-119, 1972.

Atchison, F., Sapllation and fission in heavy metal nuclei under medium energy proton bombardement, paper presented at Meeting on Targets for Neutron Beam Spallation Sources, Juelich, Germany, June 25-30, 1980.

Auerbach, E.H., A-THREE: AZ general optical model code especially suited for heavy-ion calculations, Comp. Phys. Comm., 15, 165-172, 1978.

Baumgartner, S., J. Beer, J. Masarik, G. Wagner, and H.-A. Synal, Geomagnetic modulation of the ^{36}Cl flux in the Summit GRIP ice core, *Science, 279*, 1330-1332, 1998.

Beer, J., F. Joos, C. Lukasczyk, W. Mendel, J. Rodriguez, U. Siegenthaler, and R. Stellmacher, ^{10}Be as an indicator of solar variability and climate, in *The Solar Engine and Its Influence on Terrestrial Atmosphere and Climate,* edited by E. Nesme-Ribes, pp. 221-233, Springer Verlag, New York, 1994

Bhandari, N., et al., Depth and size dependence of cosmogenic nuclide production rates in stony meteoroids, *Geochim. Cosmochim. Acta, 57*, 2361-2375, 1993.

Bland, C. J., and G. Cioni, Geomagnetic cutoff rigidities in nonvertical directions, *Earth Planet. Sci. Lett., 4*, 399-405, 1968.

Blinov, A., The dependence of cosmogenic isotope production rate on solar activity and geomagnetic field variations, in *Secular Solar and Geomagnetic Variations in the last 10,000 Years*, edited by F. R. Stephenson and A. W. Wolfendale, pp. 329-340, Kluwer Acad.,Norwell, Mass., 1988.

Bodemann, R., et al., Production of residual nuclei by proton-induced reactions on C, N, O, Mg, Al, and Si, *Nucl. Instrum. Methods Phys. Res., B82*, 9-31, 1993.

Briesmeister, J. F., MCNP - A general Monte Carlo N-particle transport code version 4A, *LA-12625-M*, 693 pp., Los Azlamos Natl. Lab., Los Alamos, N.M., 1993.

Brun, B., et al., GEANT3 User's guide, *Rep. DD/EE/84-1*, 584 pp., Eur. Org. for Nucl. Res., Geneva, 1987.

Cameron, A.G.W., A revised semiempirical mass formula, *Can. J. Phys., 35*, 1021-1031, 1957.

Carmichael, H., and M. Bercovitch, Analysis of IQSY cosmic-ray survey measurements, *Can. J. Phys., 47*, 2073-2093, 1969.

Castagnoli, G. C., and D. Lal, Solar modulation effects in terrestrial production of carbon 14, *Radiocarbon, 22*, 133-158, 1980.

Champion, K. S. W., A. E. Cole, and A. J. Kantor, Standard and reference atmosphere, in *Handbook of Geophysics and the Space Environment*, edited by A. S. Jursa, pp. 14-1 - 14-43, Air Force Geophys. Lab., Bedford, Mass., 1985.

profile in Greenland ice core from AD 1265 to 1865, *Radiocarbon, 31*, 585-591, 1989.

Damon, P. E., J. C. Lerman, and A. Long, Temporal fluctuations of atmospheric ^{14}C: Causal factors and applications, *Ann. Rev. Earth Planet. Sci., 6*, 457-494, 1978.

Garcia-Munoz, M., G. M. Mason, and J. A. Simpson, New aspects of the cosmic ray modulation in 1974-1975 near solar minimum, *Astrophys. J., 213*, 263-268, 1977.

Gosse, J. C., R. C. Reedy, C. D. Harrington, and J. Poths, Overview of the workshop on secular variations in production rates of cosmogenic nuclides on Earth, *Radiocarbon, 38*, 135-147, 1996.

Guyodo, Y. and J.-P. Valet, Relative variations in geomagnetic intensity from sedimentary records: The past 200,000 years, *Earth Planet. Sci. Lett. 143*, 23-36, 1996.

Hess, W. N., E. H. Canfield, and R. E. Lingenfelter, Cosmic ray demography, *J. Geophys. Res., 66*, 665-677, 1961.

Huggle, D., et al., Production of cosmogenic ^{36}Cl on atmospheric argon, *Planet. Space Sci., 44*, 147-151, 1996.

Hughes, E. B., and P. L. Marsden, Response of a standard IGY neutron monitor, *J. Geophys. Res., 71*, 1435-1449, 1966.

Knies, D. L., et al., ^{7}Be, ^{10}Be, and ^{36}Cl in precipitation, *Nucl. Instrum. Methods Phys. Res., B92*, 340-344, 1994.

Lal, D., Theoretically expected variations in the terrestrial cosmic-ray production of isotopes, in *Solar-Terrestrial Relationships*, edited by G.C. Castagnoli and D. Lal, pp. 216-233, Soc. Italiana di Fisica-Bologna-Italy, Bologna, 1988.

Lal, D., and B. Peters, Cosmic ray produced radioactivity on the Earth, in *Handbuch der Physik, vol. No. XLVI/2*, pp. 551-612, Springer Verlag, New York, 1967.

Light, E. S., M. Merker, H. J. Vershell, R. B. Mendel, and S. A. Korff, Time-dependent worldwide distribution of atmospheric neutrons and of their products, 2, Calculations, *J. Geophys. Res., 78*, 2741-2762, 1973.

Lingenfelter, R. E., Production of carbon-14 by cosmic-ray neutrons, *Rev. Geophys., 1*, 35-55, 1963.

Masarik, J., and R. C. Reedy, Effects of bulk chemical composition on nuclide production processes in meteorites, *Geochim. Cosmochim. Acta, 58*, 5307-5317, 1994.

Masarik, J., and R. C. Reedy, Terrestrial cosmogenic-nuclide production systematic calculated from numerical simulations, *Earth Planet. Sci. Lett., 136*, 381-395, 1995.

Michel, R., et al., Simulation and modeling of the interactions of galactic protons with stony meteoroids, *Planet. Space Sci., 43*, 557-572, 1995a.

Michel, R., et al., Production of radionuclides from target elements (Z<29) by proton-induced reactions between 800 and 2600 MeV, *Nucl. Instrum. Methods Phys. Res., B103*, 183-222, 1995b.

Michel, R., et al., Cross sections for the production of residual nuclides by low- and medium-energy protons from the target elements C, N, O, Mg, Al, Si, Ca, Ti, Mn, Fe, Co, Ni, Cu, Sr, Y, Zr, Nb, Ba, and Au, *Nucl. Instrum. Methods Phys. Res., B129*, 153-193, 1997.

Monaghan, M. C., S. Krishnaswami, and K. K. Turekian, The global-average production rate of ^{10}Be, *Earth Planet. Sci. Lett., 76*, 279-287, 1985.

Nakamura, T., H. Sugita, M. Imamura, Y. Uwamino, S. Shibata, H. Nagai, M. Takehatake, and K. Kobayashi, Measurement of long-lived ^{10}Be, ^{14}C, and ^{26}Al production cross sections for 10-40 MeV neutrons by accelerator mass spectrometry, in *Nuclear Data for Science and Technology*, edited by S. M. Qaim, pp. 714-716, Springer Verlag, New York, 1992.

Neher, H. V., Cosmic ray particles that changed from 1954 to 1958 to 1965, *J. Geophys. Res., 72*, 1527-1539. 1967.

Newkirk, L. L., Calculation of low-energy neutron flux in the atmosphere by the S_n method, *J. Geophys. Res., 68*, 1825-1839, 1963.

Nir, A., S. T. Kruger, R. E. Lingenfelter, and E. J. Flamm, Natural tritium, *Rev. Geophys., 4*, 441-456, 1966.

O'Brien, K., Secular variations in the production of cosmogenic isotopes in the Earth's atmosphere, *J. Geophys. Res., 84*, 423-431, 1979.

O'Brien, K., H. A. Sandmeier, G. E. Hansen, and J. E. Campbell, Cosmic-ray induced neutron background sources and fluxes for geometries of air over water, ground, iron, and aluminum, *J. Geophys. Res., 83*, 114-120, 1978.

Oeschger, H., J. Houtermann, H. Loosli, and M. Wahlen, The constancy of cosmic radiation from isotope studies in meteorites and on the Earth, in *Radiocarbon Variations and Absolute Chronology*, edited by I. U. Olsen, John Wiley, New York, 1969.

Parrat, Y., W. Hajdas, U. Baltensperger, H.-A. Synal, P. W. Kubik, M. Suter, and H. W. Gaeggeler, Cross section measurements of proton induced reactions using a gas target, *Nucl. Instrum. Methods Phys. Res., B113*, 470-473, 1996.

Prael, R. E., and H. Lichtenstein, User guide to LCS: The LAHET Code System, *LA-UR-89-3014*, 76 pp., Los Alamos Nat. Lab., Los Alamos, N.M., 1989.

Raisbeck, G. M., and F. Yiou, The application of nuclear cross section measurements to spallation reactions of cosmic rays, in *Spallation Nuclear Reactions and their Applications*, edited by B. S. P. Shen and M. Merker, pp. 83-101, D.Reidel, Norwell, Mass., 1976.

Raisbeck, G. M., F. Yiou, M. Fruneau, J. M. Loiseaux, M. Lieuvin, and J. C. Ravel, Cosmogenic $^{10}Be/^{7}Be$ as a probe of atmospheric transport processes, *Geophys. Res. Lett., 8*, 1015-1018, 1981.

Reedy, R. C., Nuclide production by primary-ray protons, *Proc. Lunar Planet. Sci. Conf., 17th*, Part 2, *J. Geophys. Res., 92*, suppl., E697-E702, 1987.

Reedy, R. C., and J. Masarik, Cosmogenic-nuclide depth profiles in the lunar surface (abstract), *Lunar. Planet. Sci., XXV*, 1119-1120, 1994.

Reedy, R. C., J. Masarik, K. Nishiizumi, J. R. Arnold, R. C. Finkel, M. W. Caffee, J. Southon, A. J. T. Jull, and D. J. Donahue, Cosmogenic radionuclide profiles in Knyahinya: New measurements and models (abstract), *Lunar. Planet. Sci., XXIV*, 1195-1196, 1993.

Reyss, J.-L., Y. Yokoyama, and F. Guichard, Production cross sections of ^{26}Al, ^{22}Na, ^{7}Be from argon and of ^{10}Be, ^{7}Be from nitrogen: Implications for production rates of ^{26}Al and ^{10}Be in the atmosphere, *Earth Planet. Sci. Lett., 53*, 203-210, 1981.

Schiekel, T., , U. Herpers, M. Gloris, I. Leya, R. Michel, B. Ditrich-Hanne, H.-A. Synal, M. Suter, and P. W. Kubik, Production of radionuclides from target elements (Z<30) by proton-induced reactions between 200 and 400 MeV, *Nucl. Instrum. Methods Phys. Res., B114*, 91-119, 1996a.

Schiekel, T., F. Sudbrock, U. Herpers, M. Gloris, I. Leya, R. Michel, H.-A. Synal, and M. Suter, On the production of ^{36}Cl by high energy protons in thin and thick targets, *Nucl. Instrum. Methods Phys. Res., B113*, 484-489, 1996b.

Shea, M. A., and D. F. Smart, World grid of calculated cosmic ray veryical cutoff rigidities for 1980.0, *Conf. Pap. Int. Cosmic Ray Conf.18th, 5*, 514-517, 1983.

Shea, M. A., and D. F. Smart, Recent and historical solar proton events, *Radiocarbon, 34*, 255-262, 1992.

Simpson, J. A., Elemental and isotopic composition of the galactic cosmic rays, *Ann. Rev. Nucl. Part. Sci., 33*, 323-381, 1983.

Svensmark, H., and E. Friis-Christensen, Variation of cosmic ray flux and global cloud coverage - A missing link in solar-climate relationships, *J. Atmos. Sol.. Terr. Phys,. 59*, 225-1232, 1997.

Tauxe, L., Sedimentary records of relative paleointensity of the geomagnetic field: Theory and practice, *Rev. Geophys., 31*, 319-354, 1993.

Tinsley, B. A, et al., Solar variability influences on weather and climate: Possible connections through cosmic ray Ffuxes and storm intensification, *J. Geophys. Res.* 94, 14,783-14,792, 1989.

Vogt, S., G. F. Herzog, and R. C. Reedy, Cosmogenic nuclides in extraterrestrial materials, *Rev. Geophys., 28*, 253-275, 1990.

Wilson, J.W., and C.M. Costner, Nucleon and heavy-ion total and absorption cross section for selected nuclei, NASA TN D-8107, 124 pp., NASA Langley Res. Cent., Hampton, Va., 1975.

Yiou, F., G., ^{10}Be in the GRIP ice core at Summit Greenland, *J. Geophys. Res., 102*, 26,783-26,794, 1997.

J. Beer, Environmental Physics, EAWAG, CH-8600 Duebendorf, Switzerland (e-mail: beer§eawag.ch)

J. Masarik, Space Science Laboratory, UC Berkeley, Berkeley, CA 94720-7450, USA (e-mail: masarik@ssl.berekely.edu)